Broadband/Multiband Conformal Circular Beam-Steering Array

Johnson J. H. Wang, *Life Fellow, IEEE*, David J. Triplett, and Chris J. Stevens, *Member, IEEE*

***Abstract*—A new approach for a broadband/multiband conformal circular beam-steering array is presented with both theory and experimental data. The array is low-profile, suitable for conformal mounting on a platform. It has an omnidirectional coverage with a unidirectional beam that aims at a moderate directivity of 5 to 15 dBi. It consists of a center driven element and parasitic surface waveguide elements symmetrically positioned in the periphery, for electronic beam steering and beam forming to enhance RF connectivity and/or spectral efficiency. This array can achieve ultrawideband multiband performance and low-profile conformability unattainable by conventional array approaches. In addition, its cost is estimated to be an order of magnitude lower than that of conventional beam-steering arrays. Breadboard and brassboard development efforts for the array have essentially achieved a bandwidth of 1.0–2.5 GHz. A larger bandwidth is feasible since its driven element has achieved a continuous 10:1 bandwidth, and since the surface waveguide elements could achieve a multioctave bandwidth similar to the broadbanding path from the Yagi-Uda array to the LP array.**

***Index Terms*—Arrays, beam steering, circular arrays, conformal antennas, multifrequency antennas.**

I. Introduction

THERE is a growing need for broadband/multiband beam-steering antennas driven by applications such as the software radio and WLAN (Wireless Local Area Network), among others. In these applications, steerable beams with a directivity of 5–15 dBi and omnidirectional coverage in the azimuth plane are often desired (e.g., [1]). Smart antennas with adaptive beamforming are used in WLAN and other applications not only to enhance RF connectivity by increasing signal-to-noise ratio and resilience to interferences, but also to increase spectral efficiency to overcome the inherent limitation of RF spectrum in the air. The array presented in this paper aims not only at the performance described above, but also to be broadband/multiband, covering 1–2.5 GHz or more, and be conformable for mounting on a moving platform. As such, they must have a low profile and be suitable for mounting on certain limited locations, such as the top or bottom surface, on the platform. Furthermore, cost is generally a major consideration in this and other applications.

Beam-steering arrays can be generally classified as: (1) phased arrays, (2) switched-element arrays, and (3) parasitic arrays. Past and existing antenna arrays are mostly of the phased type, with a few of the switched-element type. Unfortunately, these two types, especially the phased arrays, are expensive, bulky, and complex; though extensively researched, few of them have been deployed. These problems are also amply reflected at the component level (e.g., [2]).

The third type, the parasitic array, but without beam steering, has been widely used for four decades mainly due to its low cost. To achieve beam steering, a circular beam-steering parasitic array had been originally patented by Yagi [3], and its low-cost merits have been recognized and explored by many (e.g., [1]). However, to date they are invariably narrowband, typically employing monopole antennas as the driven and parasitic array elements. In addition, they have a high profile resulting from the use of resonant monopoles for both driven and parasitic elements.

This paper presents a beam-steering array antenna of the third type, a circular parasitic array which is broadband/multiband and low-profile. Although it evolved from the initial concept of Yagi [3], its principle is significantly different. The approach has been disclosed in a recent patent [4], with additional results presented recently in a symposium paper [5]. This paper will discuss the design approach, the theory, experimental data, as well as the practical advantages of this new beam-steering array design.

II. Broadband Low-Profile Circular Traveling-Wave (TW) Beam-steering Array

The present array aims at broadband/multiband performance for an electronically steered beam, with or without the feature of adaptive beamforming, for full 360° azimuth coverage. The array is low-profile and conformable, suitable for mounting on the top or bottom of a platform, such as a helicopter or airplane. The present array consists of a single driven element antenna in the center and multiple electronically controlled surface waveguide elements that are concentrically and symmetrically positioned around the driven element. Fig. 1 shows the top and side views of the design concept. The circular beam-steering array has a height of h_λ and diameter of D_λ, where λ is the wavelength at the lowest operating frequency.

The array is designed for conformal mounting on the top or bottom surface (conducting ground plane) of a platform to generate a directional beam electronically steered in the $x-y$ plane for 360° omnidirectional azimuth coverage. The array is small and low-profile, generally 0.085 λ to 0.17 λ high. For effective radiation, D_λ must be large enough to accommodate the radiation zones, which will be discussed in Section III-B.

Without loss of generality, the theory of operation can be explained by considering the transmit case; the receive case is similar in light of reciprocity. In Fig. 1, a TW is emitted from the center of the driven TW element antenna and propagates along,

Manuscript received April 11, 2005; revised May 2, 2006. This work was supported in part by the U.S. Army SBIR program under Contract W15P7T-04-C-L403 sponsored by U.S. Army CECOM, Ft. Monmouth, NJ.

The authors are with Wang Electro-Opto Corporation, Marietta, GA 30067 USA (e-mail: jjhwang@weo.com).

Color version of Fig. 1 is available online at http://ieeexplore.ieee.org.

Digital Object Identifier 10.1109/TAP.2006.884219

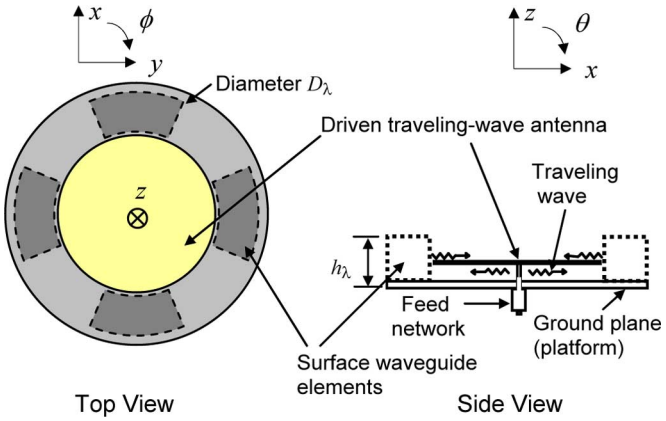

Fig. 1. Broadband/multiband beam-steering circular TW array.

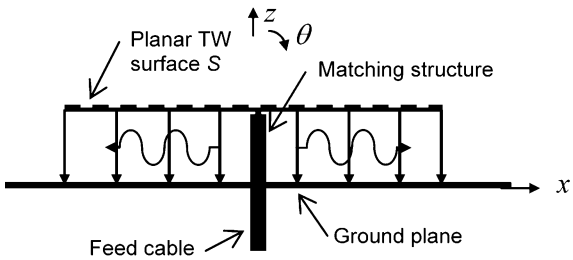

Fig. 2. The center driven TW antenna.

and intimately bound to, the ground plane as well as the TW structure.

The surface waveguide elements shown in Fig. 1 are, in essence, switchable filters which pass or reflect the incoming traveling wave. The filtering action is governed by control circuits, not shown in Fig. 1, which can vary the impedance state of each surface waveguide element. Each surface waveguide element presents two possible states to the TW, which pass or reflect the incoming TW, and thus steer the array beam. The simplicity of this array design leads to a tremendous low-cost advantage. Further information is available in a recently awarded patent [4].

Analogous to the enormous success in broadbanding linear Yagi-Uda arrays over the last eight decades, the present array should be able to achieve ultrawideband performance far surpassing the bandwidth of resonant parasitic arrays. This observation is based on their similarity in moving from a resonant structure to a TW structure, and is being confirmed by broadband data presented in this paper.

The center driven element, surface waveguide elements, electronic switching, and beam-steering computer (BSC) are discussed in detail in the following sections.

III. The Driven Center Element of the Array

A. The Ultrawideband Traveling Wave (TW) Antenna

The driven center element of the array is an ultrawideband omnidirectional traveling-wave (TW) antenna, as depicted in Fig. 2. Although the TW antenna had been extensively covered by Walter in 1965 [6], its precise definition and its inherent broadband nature were only recently elaborated by the senior author [7], with a sharper focus.

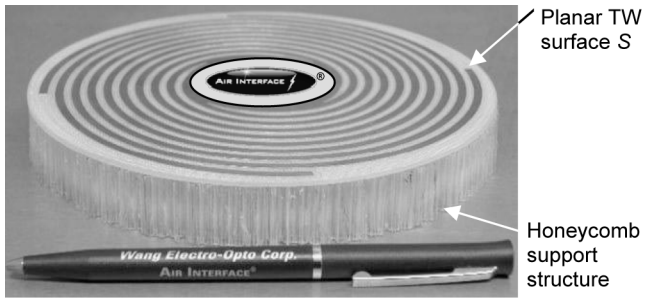

Fig. 3. Photograph of a mode-0 SMM antenna.

Both mode-0 SMM (spiral-mode microstrip) antennas [7], [8], [9] and mode-0 slow-wave antennas [9], [10] have been used in this design. For the convenience of the present discussion, we will focus on the design based on the SMM antenna, which has a low profile and an ultrawideband omnidirectional pattern bandwidth amply suitable for the present application.

Fig. 3 shows a photograph for mode-0 SMM antenna used here. The spiral structure is supported and spaced a distance above a generally planar ground surface by a low-dielectric structure, such as the honeycomb spacer shown here.

The mode-0 spiral is the case in which all the spiral arms are excited in the same phase and amplitude. The planar structure S is preferably self-complementary, in this case a self-complementary multi-arm spiral. It is also desirable that a TW has been successfully launched and maintained; under this assumption the equivalent surface currents can be readily derived from a simple TW theory in closed form since the source and fields are sufficiently decoupled. Approximate antenna properties, including gain pattern and impedance, can be obtained under these assumptions.

The multi-arm spiral planar TW surface is equivalent to an array of concentric annular slots. Thus, the antenna's radiated fields can be considered to be the superposition of the contributing fields from these concentric annular slots along ρ and a circular slot at the edge of S. This approximation of a spiral TW antenna by an array of concentric annular slots has been recently presented by the senior author [7], [11]. This approach is both physically and mathematically significant and useful, and we will take advantage of this relevance by examining the annular slot first.

B. The Mode-0 SMM Antenna as an Array of Concentric Annular Slots Plus Edge Slot

To treat the mode-0 SMM antenna as an array of concentric circular annular slots, plus a circular slot at the rim of S, we will first formulate the problem for the circular annular slot *per se* as depicted in Fig. 4. For the convenience of this discussion, the annular slot is assumed to be on the $x-y$ plane, with a radius a at the center line of the slot. The slot, of width δ, is excited by a uniform radial electric field E parallel to the ρ axis of the cylindrical coordinate system, with a resulting voltage $V(V=\delta E)$ across the slot aperture.

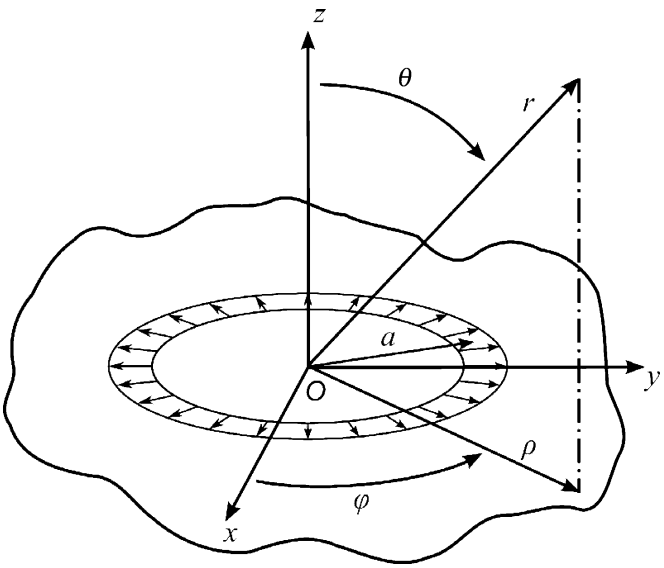

Fig. 4. An annular slot on x-y plane.

It can be shown that the far-zone radiation of a thin (small δ/λ) annular slot is fully represented by a magnetic field having only a ϕ component, as follows [9]:

$$H_\phi(\phi) = \frac{jaV\exp(-jkr)}{120\pi\lambda r}\int_0^{2\pi}\cos(\phi-\phi') \times \exp[jka\,\sin\theta\cos(\phi-\phi')]\,d\phi' \quad (1)$$

where the primed and unprimed coordinates refer to the source and field points, $\boldsymbol{r}$ and $\boldsymbol{r}$', respectively; $r = |\boldsymbol{r}-\boldsymbol{r'}|$. In this paper, the rationalized MKS system of units is used, and the $e^{j\omega t}$ convention is taken. Note here that "120π" in (1) can be more accurately represented by the free-space intrinsic (wave) impedance z_0, or $\mathrm{sqrt}(\mu_0/\epsilon_0)$, where ε_0 and μ_0 denote the free-space permittivity and permeability, respectively. The integral in (1) can be evaluated exactly, yielding

$$H_\phi = \frac{-aV\exp(-jkr)}{60\lambda r}J_1(ka\sin\theta) \quad (2)$$

where J_1 denotes a Bessel function of the first kind of order 1.

For a slot of a small diameter $(a \leq \lambda/(2\pi))$, (2) can be approximated by

$$H_\phi \cong \frac{-V\exp(-jkr)}{60r}\frac{A}{\lambda^2}\sin\theta \quad (3)$$

where $A = \pi a^2$.

Although the theory for far-zone radiated fields of a thin circular annular slot with uniform aperture excitation have been known for over half a century, they have been formally reported, to the best of our knowledge, only in the antenna handbook [12] and the original paper [13]. Unfortunately, the results in both references, in the form of (1)–(3), have some errors. Although the senior author has recently presented the corrected equations in symposiums [9], [14], it is desirable to formally publish the key equations here and to facilitate the present discussion.

It is worth pointing out that (2) and (3) can be verified independently by invoking duality from the case of a circular electric loop antenna based on Maxwell's equations having full-fledged presentation of magnetic sources [15]. This derivation, though straightforward, could have been used to detect the errors in [12] without going through the difficult direct derivation which involves advanced electromagnetic theory and mathematics.

The far-zone radiated magnetic field of the mode-0 SMM antenna, as an array of concentric annular slots, consists of a ϕ component only and is given by

$$H = H_\phi = \sum_{\ell=1}^{\ell=N} H_\ell(\theta,\phi) = \sum_{\ell=1}^{\ell=N}\frac{-a_\ell V_\ell\exp(-jkr)}{60\lambda r}J_1(ka_\ell\sin\theta)e^{j\psi_\ell} \quad (4)$$

where ψ_ℓ and V_ℓ denote, respectively, the phase and amplitude of the voltage of annular slot element ℓ located at a radial distance $\rho = a_\ell$.

The series in (4) can be approximately evaluated by the method of stationary phase by including only a few terms with in-phase contribution. Physically, this means including only annular slots in the "radiation zones." For a 2-arm mode-0 spiral, the radiation zones are at circumferences where the phase change $\Delta\psi_J$ equals $\pi/2$ between adjacent arms so that an equivalent annular slot is formed over two rings of adjacent annular slots, with a resulting voltage V across it. For a 4-arm mode-0 spiral, $\Delta\psi_J = \pi/4$ between adjacent arms at the radiation zone; four adjacent slots are needed to form an equivalent annular slot. Thus, the radiation zones are at circumferential rings with radii ρ_r given by [9]

$$\rho_r = \lambda/(4\pi) + n\lambda/\pi \text{ for } 2-\text{arm spiral} \quad (5a)$$

$$\rho_r = \lambda/(8\pi) + n\lambda/\pi \text{ for } 4-\text{arm spiral} \quad (5b)$$

where $n = 0, 1, 2, 3\ldots$

It is noteworthy that the present theory is in closed form, thus readily provides physical insights without the need for numerical analysis that often clouds the physics involved. As a result, the design optimization process can be carried out efficiently. Later we will present some computed data and compare them with the theory.

C. Impedance Matching for the TW Antenna

The planar TW surface S can be considered a loaded surface consisting of both a reactive component and a resistive component, the latter accounting for possible radiation through the nonconducting (slot) region. At the rim of S, a circular slot radiates the residual power as discussed in the preceding subsection.

In regions where the planar structure S is a solid conductor, the TW structure can be viewed as a circular radial waveguide of height h, with its characteristic impedance Z_{00} at ρ for the $m = n = 0$ mode given by

$$Z_{00} = (z_0/2\pi)h/\rho \sim 60h/\rho. \quad (6)$$

Note that Z_{00} changes with the distance from the center of the radial waveguide, yet is independent of frequency.

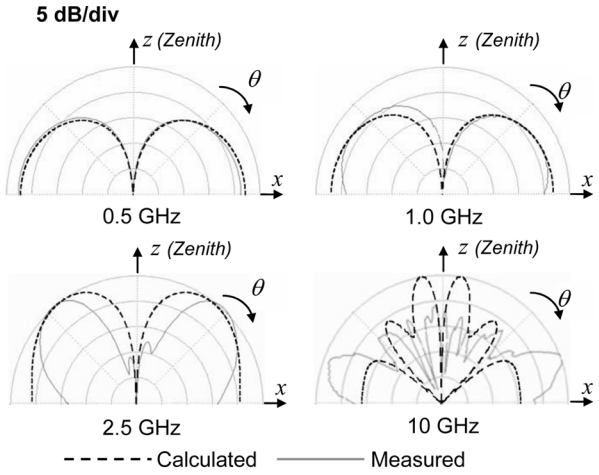

Fig. 5. Comparison between computed and measured elevation radiation patterns.

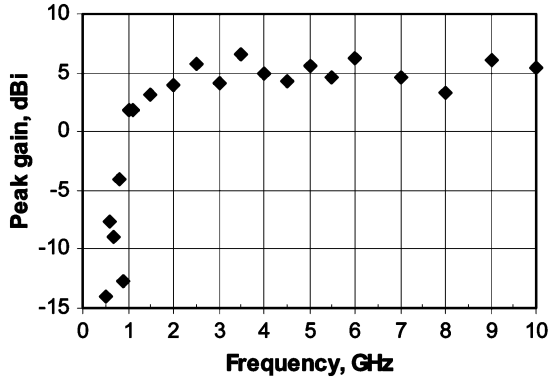

Fig. 6. Measured gain of mode-0 SMM antenna.

In regions where S is self-complementary and higher-order modes are suppressed, the characteristic impedance Z_c is

$$Z_c \sim 2Z_{00}. \tag{7}$$

Equation (7) is based on the self-complementary geometry of the planar TW surface S and the principle of duality inherent in Maxwell equations having full-fledged presentation of magnetic sources [15].

Equations (6) and (7) are consistent with our empirical observations. They provide the basis for ultrawideband impedance matching under the condition that higher-order modes are suppressed. Indeed, excellent impedance matching over a 10:1 bandwidth (1–10 GHz) has been achieved, with $\mathrm{SWR} < 1.3$ mostly, rising to <2.0 only at high and low frequencies, as has been presented in a symposium paper [8].

D. Gain Pattern Performance of the Center Driven Element

Several mode-0 SMM antenna breadboard models, each about 14.5 cm in diameter and 2.69 cm in height, mounted on a conducting ground plane of 30.5 cm diameter, were designed, fabricated, and tested successfully.

Fig. 5 exemplifies a comparison between computed and measured elevation radiation patterns over 0.5–10.0 GHz. As can be seen, the agreement between theory and measured data is very good at the lower frequencies, but gradually deteriorates as the frequency increases. Obviously, the theoretical model which assumes no higher-order modes deviates more and more from reality as the frequency increases. In fact, at 10 GHz the height of the radial waveguide is about 1 free-space wavelength, the TW can no longer be tightly bound to the microstrip-line mode, and the radiation of the edge at the rim of S becomes significant.

Fig. 6 shows the measured gain (at the beam peak) of the mode-0 SMM antenna over the frequency range of 0.5–10 GHz. As can be seen, the antenna has a 10:1 gain bandwidth (over 1.0–10 GHz) with a minimum gain of 1 dBi. The measurement was conducted at an anechoic chamber of Wang Electro-Opto Corporation and calibrated against standard gain antennas. This antenna has also been measured by the U.S. Army Communications-Electronics Research Development & Engineering Center (CERDEC) at Ft. Monmouth, NJ. CERDEC personnel in its Antennas & Ancillaries Branch measured the antenna's performance in their anechoic chamber over a frequency range of 1–8 GHz, and obtained results which generally confirm our measured data as presented here.

As has been discussed in the paper, the mode-0 SMM antenna generally acts as a traveling wave antenna. As the frequency is lowered below 1 GHz, however, the antenna eventually becomes too small to adequately support the traveling wave, and resonance phenomena take over, resulting in the narrowband peaks and dips in gain as seen in Fig. 6.

IV. Parasitic Surface Waveguide Elements

For the TW array as depicted in Fig. 1, in order to achieve beam-steering over the desired frequency range, surface waveguide elements employed in this array must function, over broad frequency bands, as either a passband filter or a band reject filter depending on their individual switching states. Alternatively, or equivalently, the TW structure can be viewed as a leaky radial transmission line that supports a TW in a selected direction while suppressing propagation in other angular directions.

Both impedance matching and frequency/spatial filtering theory are applied to the present microwave structures since their apparent differences are merely from a utilitarian point of view. Here we take advantage of this unified concept in order to benefit from the extensive knowledge and insight in these apparently diverse fields to facilitate the design work.

This TW concept is obviously different from the resonant director and reflector functions that the parasitic elements perform in the Yagi array [1], [3], which are inherently narrowband resonant antennas. That broadband surface waveguides, instead of conventional resonant parasitic elements, are used here is a foundation for the broadband/multiband performance of this circular array.

The passive array elements surrounding the center driven element act as variable filters which pass or reflect the incoming traveling wave. The filtering states of the passive elements are governed by a control circuit, thus providing electronic steering of the array. These surface waveguides are filters made of distributed elements, versus filters made of lumped elements at lower frequencies, and are a section of the transmission line supporting the traveling wave.

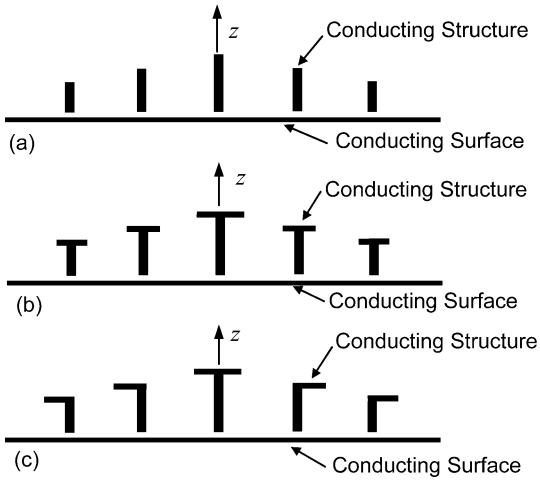

Fig. 7. Surface waveguides consisting of a set of conducting plates, rods, or a corrugated structure above a conducting surface.

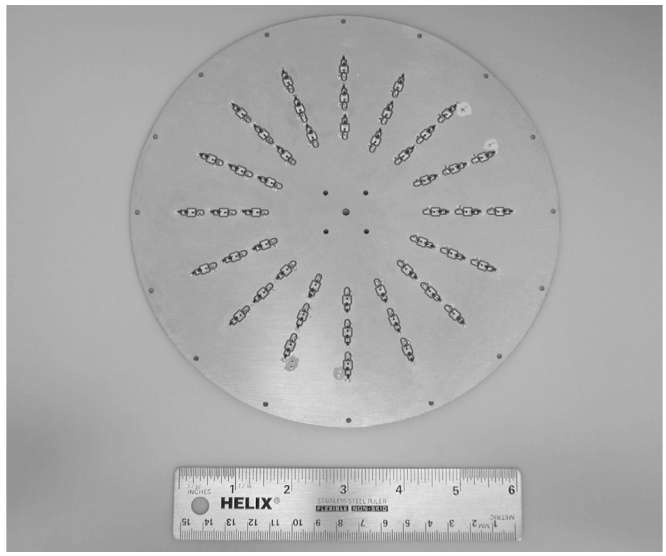

Fig. 8. Brassboard RF switching circuit utilizing PIN diodes.

The broadband/multiband feature of these surface waveguides is rooted in the physics of the surface wave which can be supported on a generally planar and preferably reactive surface. Fig. 7 shows some surface waveguides consisting of a set of conducting plates, rods, or a corrugated structure above a conducting surface [4]. These discrete structures, as well as continuous structures, are means to implement switchable surface waveguide structures in practical arrays.

A surface wave is also supported on a purely conducting and essentially planar surface [16]. The surface waveguide can support a surface wave with no low-frequency cutoff, and has only a minimal number of discrete modes. The selection of the surface waveguide must be based on the TW that propagates in the TW structure [6].

The transverse magnetic (TM) mode has electric fields perpendicular to the plane surface and in the direction of propagation. The corrugated surface is another well known surface waveguide for the TM surface wave. Equally important is that it can either pass or reject the surface wave.

Although there are many surface wave guides, for the present application only those with variable filtering actions controllable electronically are potential candidates. Thus, the surface waveguide in Fig. 7 has binary states achieved by shorting or opening the small gap with a device such as a PIN diode, resulting in a connection or disconnection between the corrugated structure and the conducting surface.

Theory for the surface waveguides in Fig. 7 predicts broadband filtering action in both states. The filtering bandwidth of a given surface waveguide element can be expanded by the use of frequency-independent structures. For example, it can be derived from a periodic structure or a log-periodic (LP) structure. Using this technique, each surface waveguide element is a log-periodic structure with its impedance state controlled as a single unit.

There are various LP structures. For the present application, only those that are amenable to switching of their impedance states are selected for experimentation. These closely related LP structures include, but are not limited to, the zigzag antennas, the LP dipole arrays, etc.

A simple implementation is similar to that of the LP dipole array, for which the basic theory has been well established. The data for the LP dipole array can be applied to the case of the LP monopole array and used as a basis for the surface waveguide elements. This approach has the advantage of convenience in implementing control circuits for the switching of impedance states.

The broadbanding potential of such surface waveguide structures is readily envisioned in light of the historical perspective that the bandwidth of the Yagi-Uda array has expanded from about 1% in its early stage to perhaps 20:1 in the form of log-periodic arrays.

V. Electronic Switching of Surface Waveguide Elements

For the experimental models developed, each surface waveguide element has two distinct impedance states. In the first state, the surface waveguide element is shorted to the ground plane, and in the second state it is isolated from the ground plane, as indicated in Fig. 7. For ideal beam-steering the two states should represent absolute "short-circuit" and "open-circuit" conditions.

In practice, the connection or isolation from the ground plane is accomplished by an electronically-controlled switching circuit. One such practical circuit uses PIN diodes for the RF switching, and a lumped-element low-pass filter on the DC control line which biases the PIN diodes. It is essential that the circuit adequately isolates the RF energy from transfer to the control circuitry in order to maximize the effective gain of the antenna system.

A breadboard RF switching circuit using PIN diodes, as shown in Fig. 8, has been successfully designed, fabricated, and tested to demonstrate the feasibility of the approach. Over the 1–2.5 GHz range, the switching circuit has achieved isolation of >20 dB between the surface waveguide element (located above the antenna ground plane) and the control circuit (located behind the antenna ground plane). The circuit presents two distinct impedance states to both the inward and outward TW. The

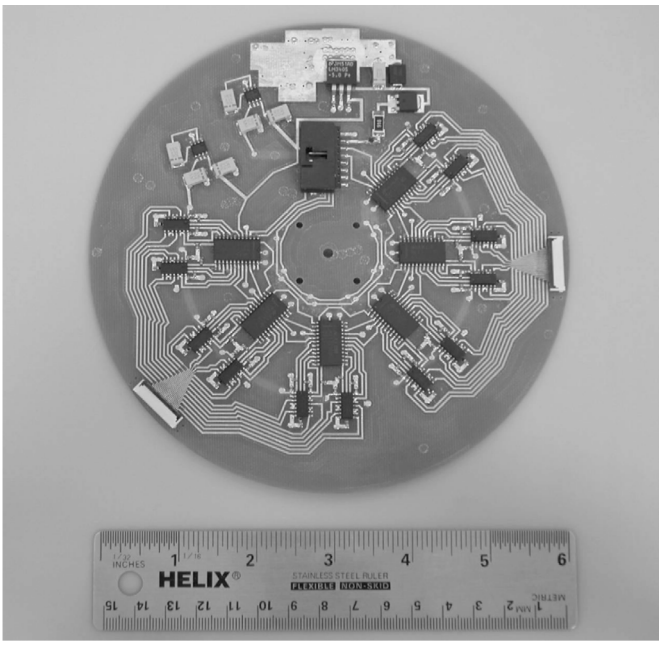

Fig. 9. Brassboard digital switching circuit for biasing PIN diodes.

circuit is also designed to have adequate impedance matching over the instantaneous bandwidths for the operation. Further information is available in the recently-awarded U.S. patent on this array [4]. The design of these circuits, though satisfactory for the present application, has not been fully optimized. For further optimization, a range of techniques are available (e.g., [17]), which will not be elaborated here.

For better RF isolation, photovoltaic Field-Effect Transistor (PV-FET) switches are probably more suitable [18]. Optically coupled control of PV-FET switches can offer a significant increase in the isolation between the RF and control circuits, and therefore improve the performance of the array system. The broadband nature of such FET switches has been previously demonstrated.

The digital control circuit is on another layer, as shown in Fig. 9. This circuit receives state information for each RF switch via a serial interface to a beam-steering computer. The circuit translates the serial data to forward or reverse bias conditions for each PIN diode in the RF circuit, and applies the appropriate bias to each PIN diode. The resulting array beam states are discussed later in Section VII.

VI. Beam-Steering Mechanisms for the Circular Traveling-Wave Array

Fig. 10 shows the block diagram for the beam-steering array for installation on a moving platform in a WLAN application. The array is a "smart antenna" that directs its beam toward another transceiver in the WLAN system under a beam-steering command. The command can be based on a signal from the targeted transceiver, or from an internally programmed input from local embedded geolocator.

A number of approaches and algorithms for beam steering in conventional phased arrays and switched-beam arrays already exist. However, since the parasitic array has a single RF port,

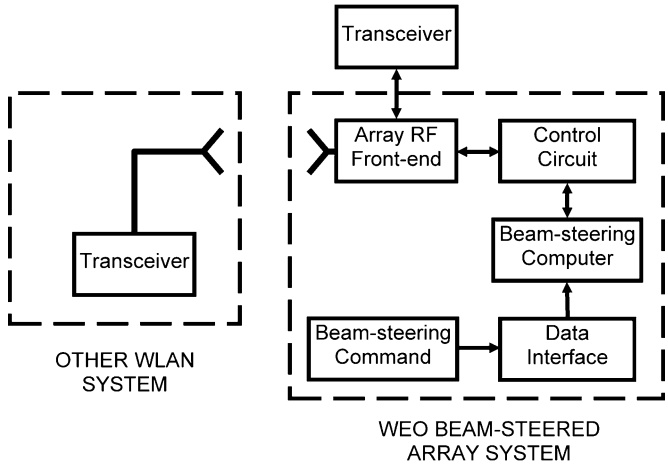

Fig. 10. System block diagram for WEO's broadband WLAN beam-steering array.

most conventional beam-steering algorithms are inadequate for it. Thus, a significant amount of research has been devoted in recent years to development of beam-steering algorithms for use in parasitic arrays (e.g., [1]).

The immediate application for the present design is on a moving platform for broadband wireless networking. There are several approaches to establish a communications link. In one approach, the array system determines the required beam-steered radiation pattern based on the positions of each node of the network. The relative positions are determined from its internal geolocation sensors embedded in each array system.

The array system uses embedded Global Positioning System (GPS) and Inertial Navigation System (INS) to determine the position and attitude of the array, which are used by the beam-steering computer along with the position of a remote array to calculate the desired beam direction. The position of each remote array is transmitted over the wireless LAN to network nodes, enabling the array to maintain a link between multiple moving platforms.

Of great significance in general is the capability of the array for adaptive beamforming. There has recently been much progress in the open literature in the application of adaptive beamforming algorithms to narrowband circular parasitic arrays, especially in the wireless LAN environment. This new broadband array is compatible with such algorithms, and can use them to further enhance its performance and cost.

VII. Breadboard Development Effort

The preceding sections presented the design of an ultrawideband/multiband circular array system as well as the enabling technologies necessary for the design approach. Breadboard and brassboard development efforts have demonstrated a 1–2.5 GHz beam-steered array. The center driven traveling-wave antenna has been well developed, as discussed earlier. Development for the beam-steering computer, the control circuit, the beam-steering command, and its data interface has been largely successful, resulting in their functionality, physical compatibility, and low-cost feature fairly well established. The broadband matching of the surface waveguide remains as the only technical difficulty.

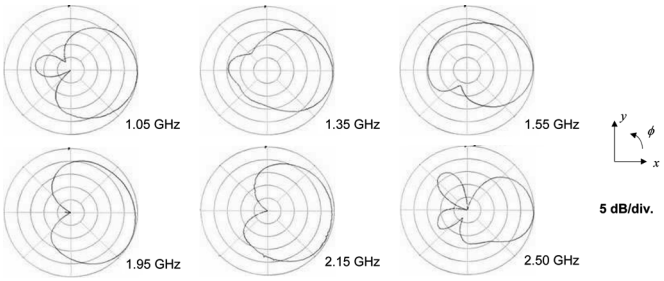

Fig. 11. Measured azimuth radiation patterns of breadboard array mounted on a 61-cm diameter ground plane.

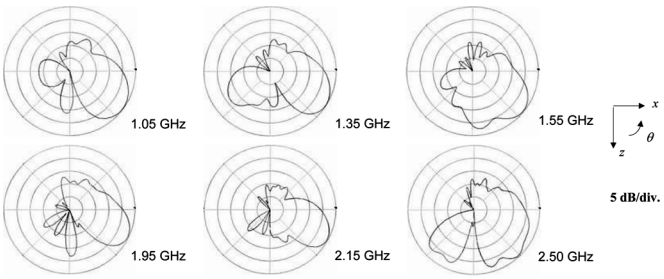

Fig. 12. Measured elevation radiation patterns of breadboard array mounted on a 61-cm diameter ground plane.

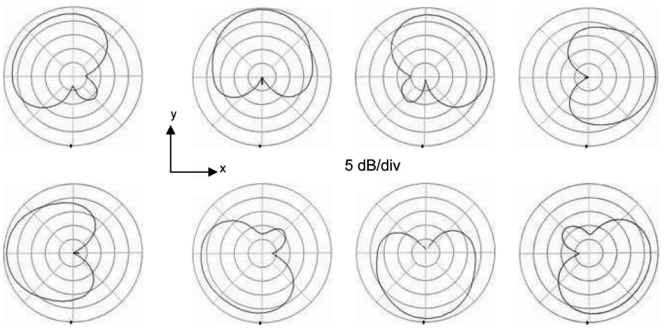

Fig. 13. Measured azimuth radiation pattern at a selected frequency, showing beam steering covering full azimuth angle of 360°.

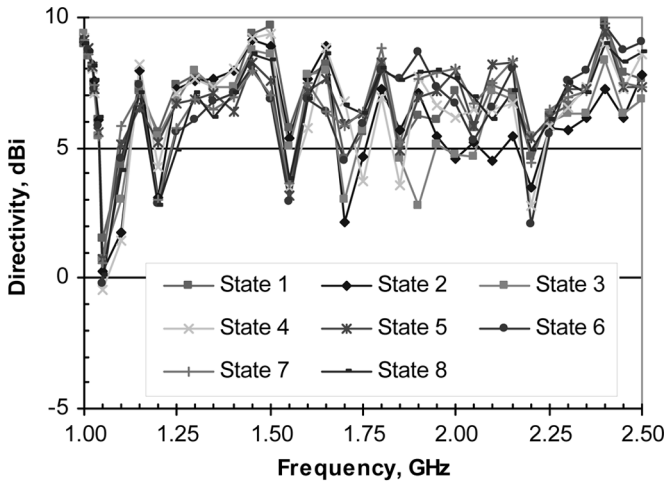

Fig. 14. Estimated directivity of the beam-steered array at the beam peak in each of the eight directional states.

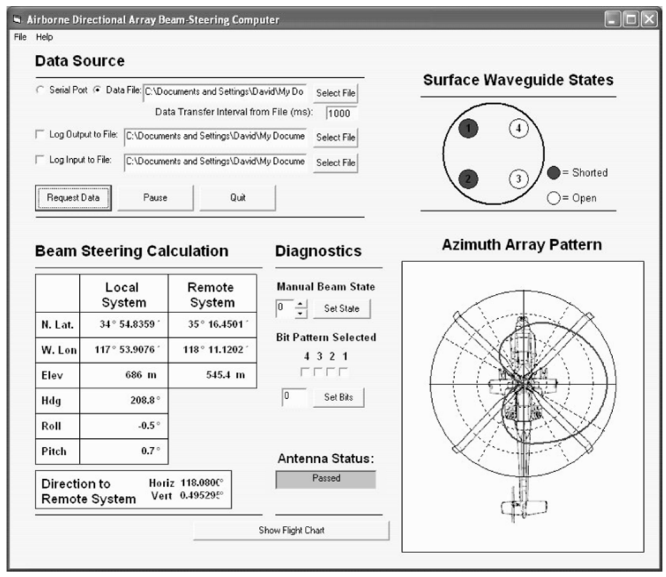

Fig. 15. Screen capture of display panel of beam-steering computer.

Breadboard array models have achieved a beam-steering bandwidth of 1.0–2.5 GHz except for two or three narrow bands of low performance. Fig. 11 shows measured azimuth patterns with a directive beam toward $\phi = 0°$, over 1.0–2.5 GHz. Fig. 12 shows measured elevation patterns with a directive beam toward $\theta = 90°$ over 1.0–2.5 GHz.

Although there is an undesirable, yet generally unavoidable, elevation beam tilt of 30° to 45°, the elevation pattern coverage over the 1–2.5 GHz bandwidth is essentially adequate. The beam-steering feature of the array is exemplified by the measured azimuth radiation patterns for eight steered beams, covering full azimuth angles over 360°, at a selected frequency, as shown in Fig. 13.

Fig. 14 shows the directivity of the breadboard array over an operating frequency range of 1–2.5 GHz as well as instantaneous bandwidths of 20–200 MHz. And we expect to broaden both bandwidth greatly. This model has a directivity generally between 5 and 8 dBi. The losses, and thus the reduction in gain, are estimated to be between 1.5 and 4 dB, depending on the frequency. The losses are mainly due to impedance mismatch, which will be reduced as the research continues. Another model under development aims at a directivity of 10 dBi.

Fig. 15 is a photograph showing the dynamic feature of the array on the display panel of its beam-steering computer (BSC). The array has a manual mode and an automatic mode. The display panel of the BSC shows several key features of the beam steering in real time, which are useful for the operator as well as the engineer at this development stage.

As can be seen, the pattern displayed shows a directional beam with a directivity of about 5 dBi, as needed for this specific application. For applications aimed at maximizing the spectral efficiency, increasing capacity, or achieving robust and reliable connectivity, beams of this smart antenna can also be formed adaptively to maximize the signal-to-noise ratio, with pattern nulls formed in the directions of interferences.

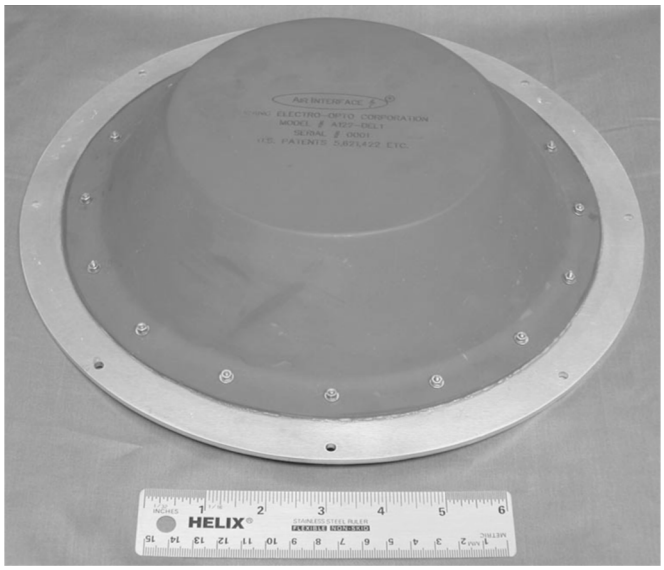

Fig. 16. A brassboard model of the circular beam-steering array.

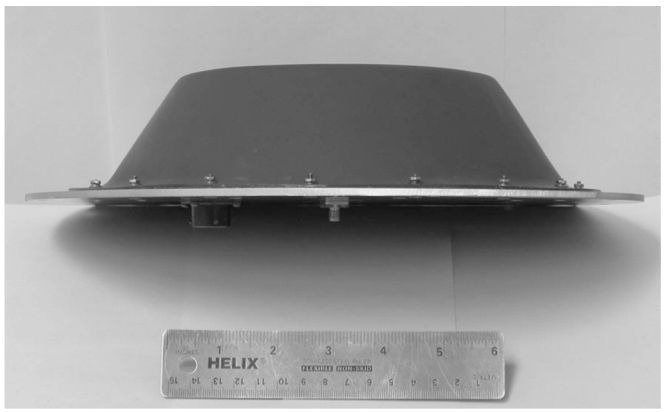

Fig. 17. Side view of a brassboard model of the circular beam-steering array.

VIII. Size, Shape, Weight, Conformability, Cost, Etc.

As discussed in the introduction section, this beam-steering array antenna is aimed at practical applications on moving platforms. Therefore, in addition to broadband/multiband performance, it must be small, low-profile, light-weight, and rugged, suitable for mounting on ground and airborne vehicles. Earlier research at Wang Electro-Opto Corporation using conventional phased array and switched-element array techniques had encountered severe difficulties in meeting these requirements. Perhaps more significantly, conventional approaches are much more costly and complex than the present approach.

Fig. 16 shows a photograph of a brassboard 1–2.5 GHz model of the entire circular beam-steering array, protected by a radome, with its beam-steering computer excluded from the photo, in contrast with a 15 cm (6 inch) ruler. (All the array radiating structure, control circuits, data interface, etc. are contained in the structure between the aluminum mounting plate and the fiberglass radome.) Fig. 17 shows a side view of the brassboard model. Visible in Fig. 17 are the connector for the array control interface (off center) and the SMA connector for the RF signals (at the center). As can be seen, the small size and low-profile shape of the array are attractive in comparison with other electronic beam-steering arrays.

A cursory analysis has been performed to assess the production cost of this array. While necessarily depending on the quantities involved, the production cost for this array antenna is roughly one order of magnitude lower than that for conventional phased arrays.

The high cost of conventional phased arrays is mainly due to their beam forming at the array elements, which are at the expensive RF level. The resulting complexity and per-module cost in conventional broadband/multiband electronically steered phased arrays are of course well known. The cost problem is greatly exacerbated when the bandwidth requirement is increased to beyond 2:1 [19]. As a result, conventional broadband/multiband beam-steering phased arrays have been designed only for military and space applications, which are less sensitive to cost pressure [18].

In the present design of parasitic array, the switching is performed at frequencies much lower than the RF operating frequencies. At these low frequencies, switching circuits benefit from low-cost commercial-off-the-shelf parts.

IX. Conclusion

A new approach for a broadband/multiband conformal circular beam-steering array is presented with essential theory and experimental data. The array consists of a center driven element with continuous 1.0–10 GHz bandwidth and broadband parasitic surface waveguide elements in the periphery for beam steering. It has an omnidirectional coverage with a medium antenna gain suitable for many platform-mounted applications. Breadboard and brassboard development efforts for the array have achieved an operating bandwidth of 1.0–2.5 GHz except for two or three narrow bands of low performance, for instantaneous bandwidth of 20–200 MHz. The functionality, physical compatibility, and low-cost feature of the array design have been well demonstrated.

The array is low-profile, suitable for mounting conformally on the top or bottom of a moving platform. Such broadband feature and low-profile conformability appear unattainable by conventional arrays. Perhaps more significant is its low production cost, which is estimated to be one order of magnitude lower than that of conventional beam-steering phased arrays.

At present, the antenna's ultrawideband/multiband performance is limited mainly by the bandwidth of the surface waveguides. However, based on the successful broadbanding effort of the linear Yagi-Uda array with a bandwidth of $< 1\%$ at its inception to the 20:1 bandwidth achieved by the LP dipole array, the potential for unprecedented ultrawideband and multiband performance for the present array considerably beyond the 2.5:1 bandwidth achieved, as well as performance enhancement, is promising.

References

[1] C. Sun, A. Hirata, T. Ohira, and N. Karmakar, "Fast beamforming of electronically steerable parasitic array radiator antennas: Theory and experiment," *IEEE Trans. Antennas Propag.*, vol. 52, no. 7, pp. 1819–1832, Jul. 2004.

[2] M. B. Steer, Ed., *IEEE Trans. Microw. Theory Tech., Mini Special Issue on Radio Frequency Integrated Circuits*, p. 3, Jan. 2006.

[3] H. Yagi, "Variable Directional Electric Wave Generating Device," U.S. Patent 1 860 123, May 24, 1932.
[4] J. J. H. Wang, "Broadband/Multiband Circular Array Antenna," U.S. Patent 6 972 729, Dec. 6, 2005.
[5] J. J. H. Wang, D. J. Triplett, and C. J. Stevens, "Broadband/multiband conformal circular beam-steering array," in *Proc. IEEE Int. Microwave Symp.*, Long Beach, CA, Jun. 12–17, 2005.
[6] C. H. Walter, *Traveling Wave Antennas*. New York: McGraw-Hill, 1965.
[7] J. J. H. Wang, "The spiral as a traveling wave structure for broadband antenna applications," *Electromagn.*, pp. 20– 40, Jul.–Aug. 2000.
[8] J. J. H. Wang, C. J. Stevens, and D. J. Triplett, "Ultrawideband omnidirectional conformable low-profile mode-0 spiral-mode microstrip (SMM) antenna," in *Proc. IEEE Antennas Propagation Symp.*, Washington, DC, Jul. 3–8, 2005.
[9] J. J. H. Wang, "Theory of a class of planar frequency-independent omnidirectional traveling-wave antennas," in *Proc. IEEE Int. Symp. on Microwave, Antenna, Propagation and EMC Technologies for Wireless Communications*, Beijing, China, Aug. 8–12, 2005.
[10] ——, "Broadband Miniaturized Slow-Wave Antenna," U.S. Patent 6 137 453, Oct. 24, 2000.
[11] J. J. H. Wang, "Theory of frequency-independent antennas as traveling-wave antennas and their asymptotic solution by method of stationary phase," in *Proc. Int. Symp. Antennas and Propagation (ISAP2005)*, Seoul, Korea, Aug. 3–5, 2005, pp. 379–382.
[12] H. Jasik, Ed., *Antenna Engineering Handbook*, 1st ed. New York: McGraw-Hill, 1961.
[13] A. A. Pistolkors, "Theory of the circular diffraction antenna," in *Proc. IRE*, Jan. 1948, pp. 56–60.
[14] J. J. H. Wang, "The physical foundation, developmental history, and ultra-wideband performance of SMM (spiral-mode microstrip) antennas," in *Proc. IEEE Antennas and Propagation Symp.*, Washington, DC, Jul. 3–8, 2005.
[15] J. J. H. Wang, *Generalized Moment Methods in Electromagnetics—Formulation and Computer Solution of Integral Equations*. New York: Wiley, 1991, pp. 6–7, 105–107.
[16] R. E. Collin, *Field Theory of Guided Waves*, 2nd ed. New York: IEEE Press, 1991.
[17] G. Matthaei, L. Young, and E. M. T. Jones, *Microwave Filters, Impedance-Matching Networks, and Coupling Structures*. Norwood, MA: Artech House, 1980.
[18] J. J. H. Wang, J. K. Tillery, G. T. Thompson, K. E. Bohannan, R. M. Najafabadi, and M. A. Acree, "A multioctave-band photonically-controlled, low-profile, structurally-embedded phased array with integrated frequency-independent phase-shifter," in *Proc. IEEE Int. Symp. On Phased Array Systems and Technology*, Boston, MA, Oct. 15–18, 1996.
[19] J. J. H. Wang, "Practical methods to reduce cost and complexity of optically controlled phased arrays," presented at the IEEE MTT-S Int. Microwave Symp., Low Cost Digital and Analog OE Modules: Manufacturing and System Insertion Workshop, Baltimore, MD, Jun. 7–12, 1998, unpublished.

Johnson J. H. Wang (M'68–SM'79–F'92–LF'04) received the B.S.E.E. degree from National Taiwan University, Taipei, Taiwan, R.O.C. and the Ph.D. in electrical engineering from The Ohio State University, Columbus, in 1968.

Since 1991, he has been Chief Scientist and President of Wang Electro-Opto Corporation (WEO), Marietta, GA. From 1975 to January 1995, he was on the faculty of the Georgia Institute of Technology, Atlanta. Prior to coming to Georgia Tech in 1975, he had seven years of industrial experience in the design of various antennas and phased arrays. He is the author of a book *Generalized Moment Methods in Electromagnetics—Formulation and Computer Solution of Integral Equations* (New York: Wiley, 1991). At Georgia Tech his research was in the area of antennas, microwaves, and electromagnetic theory. A focus of his research was the computation of a variety of three-dimensional electromagnetic problems using digital computers by the method of moments. His current fields of interest are broadband/multiband low-profile conformable antennas, smart antennas. Software-defined arrays, and array antenna systems, multifunction and diversity antenna systems employing modern microwave and lightwave technologies, digital beam forming, as well as wireless telecommunications.

Dr. Wang is a Member of The Electromagnetics Academy.

David J. Triplett was born in Savannah, Georgia, on July 22, 1966. He received the B.S. degree in engineering from Georgia Institute of Technology, Atlanta, in 1993.

From 1993 to 2000, he developed various computerized control systems, and performed computer-based modeling and simulation of various electromechanical, chemical, and hydrogeological processes. In 2000, he joined Wang Electro-Opto Corporation (WEO), Marietta, GA, as an Engineer where, since 2003, he has been a Senior Engineer. At WEO, he has been actively engaged in antenna development, phased array systems simulation, and development of hardware and software for beam-steering arrays and smart antennas. He also has extensive experience in the integration of computer systems and their interface with other electrical and electromechanical systems, including both wired and wireless environments.

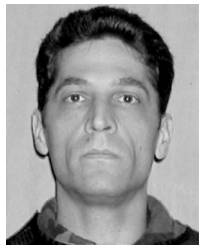

Christopher J. Stevens (M'04) was born on December 6, 1969 in Massachusetts. He received the B.S. degree in electrical engineering from the University of Massachusetts at Amherst, in 1996.

From 1988 to 1991, he was a Master Technician in the U.S. Air Force working on the ground electronics systems for the Minuteman III ICBM. Since 1996, he has conducted various engineering and design work in the area of wireless telecommunications, with focus in antenna systems. In 2002, he joined Wang Electro-Opto Corporation (WEO), Marietta, GA, where he is now a Senior Engineer.